DEFORMATION OF VISCOELASITIC DROPLETS THROUGH INERTIAL FOCUSING IN MICROFLUIDICS

by

Yuelin Chen

A thesis submitted to Johns Hopkins University in conformity with the requirements for the degree of Master of Science in Engineering

Baltimore, Maryland

May 2021

Abstract

Inertial focusing in microfluidics has been a promising method for cell sorting in recent years. Despite various experiments and applications in devices implemented for cell sorting, the mechanisms of inertial focusing of deformable particles have yet to be elucidated. Various experiments conducted in inertial focusing demonstrated that the shape and deformation of droplets would affect particle motion and their steady state focusing position. The significance of deformation in inertial focusing inspired this work. In this thesis, we would show the deformation of viscoelastic droplets under different flow rates. Our experimental results show that for dimensionless droplets size 0.2-0.4, an oval shape is formed and a simple two-dimensional measurement has been used to define a deformation of viscoelastic droplets. Analysis shows that the deformation by Taylor measurement could be estimated by the flow and droplet properties and an equation for deformation prediction would be presented. As deformation is an intrinsic factor to any deformable particle in inertial focusing, this connection would provide convenience in assessing deformation contributions in affecting focusing positions. We envision a better understanding of the mechanics of inertial focusing, leading to the improvement of microfluidic devices for cell sorting.

Acknowledgements

I would like to sincerely thank my advisor Prof. Soojung Claire Hur for her guidance and mentorship throughout my master's degree program and related research. She has been very kind and shows strong concern for my work and my academic experience at Hopkins. It's an honor to be able to work in her lab and the process is enjoyable and also rewarding.

I would also like to express sincere gratitude to Prof. Baskar for his assistance in data analysis in my project. And also Prof. Tamer Zaki for his guidance in fluid dynamics in my Master's program.

I would like to thank my roommates Fang and Dong, that is also from Hopkins. It wouldn't have been easy to live in the pandemic without the fun of living together.

Lastly, I would like to thank my parents for supporting me to study abroad in the US. They gave me love and courage throughout my life.

Table of contents

Contents

1 Inertial focusing

1.1 Inertial focusing in microfluidics

Inertial microfluidics has been inspired by the need for the motion of cells on the microscale to be under control in the biological and medical fields. Techniques including filtration [1, 2, 3, 4], cell cytometry [5, 6, 7] ,and other techniques including dielectrophoresis [8, 9, 10] resorting to external fields are alternatives means of cell separation. Among these promising technologies, inertial focusing demands small volumes of samples, and flow conditions can be precisely controlled. [11, 12]

Inertial focusing was first discovered by Serge and Silberberg [13] in macroscale tube flow where particles would migrate to a relative position to the wall infinite flow rate or Reynolds number. The specific focusing position in migration is a result of two balanced forces: the shear-gradient-induced lift force from the parabolic profile of a pressure-driven flow or Poiseuille flow and the wall-lift force that drives the particles away from the channel.

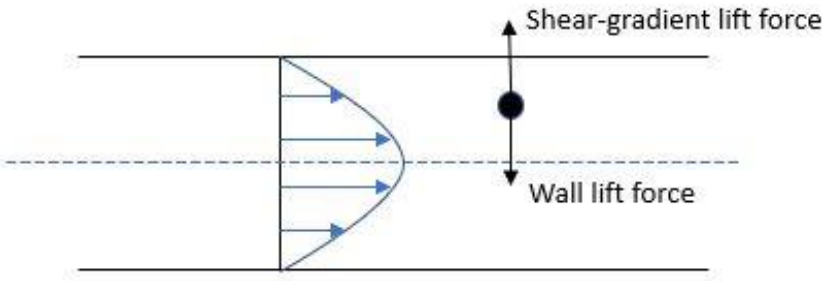

Figure 1 The two main forces in inertial focusing

Apart from annular focusing in circular tubes that are first observed, [1, 2, 14, 15] four or eight equilibrium positions in square tubes have been reported by several groups; two or four equilibrium positions have been observed in most rectangular tubes. Our deformable drops inertially focused in rectangular tubes also have two or four focusing positions depending on the experimental conditions. The fundamentals to explain like this in microfluidics are still elusive [16]. This indicates that accounting for symmetry, more than one position would the forces on the particle's balance which couldn't be fully dictated by the current understanding based on the balance of two lift forces.

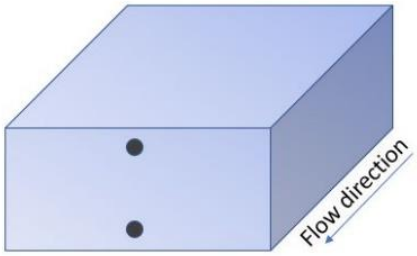

Figure 2(a) Two focusing positions in rectangular tubes

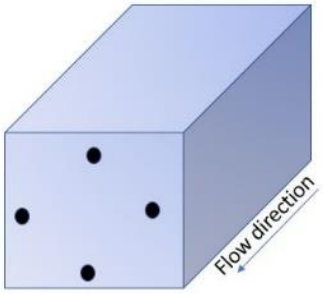

Figure 2(b) Four focusing positions in square tubes

1.2 Droplet focusing and its dependence on deformation

This research is an extension of deformation-based cell classification by Hur et al. In which Hur demonstrated that lateral equilibrium of particles relies on viscosity ratio and particle size [17]. Viscous oil capsules were controlled by choosing silicone oil with various kinematic viscosities from 1 cSt to 1000 cSt. The strong reliance of equilibrium on particle size is characterized by the increase of the curves in a nonlinear scheme with a positive second derivative. Elastic solid particles made of PDMS are experimented with to add rigid particles into comparison. The equilibrium of the rigid particles is observed to be closer to the wall than the viscous oil droplets show in figure3(a). This is associated with increased deformation-induced lift force [18, 19] due to its deformed shape in the steady state.

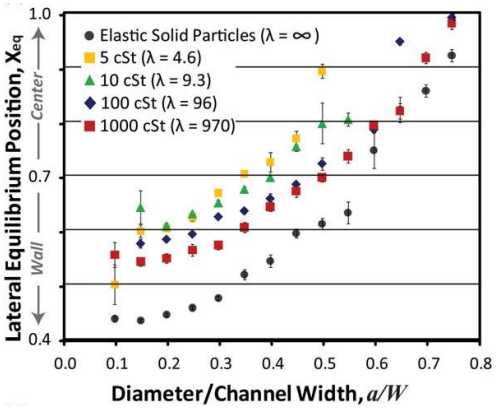

(a) Equilibrium for viscous oil droplets and elastic particles as a function of dimensionless particle size a/W.

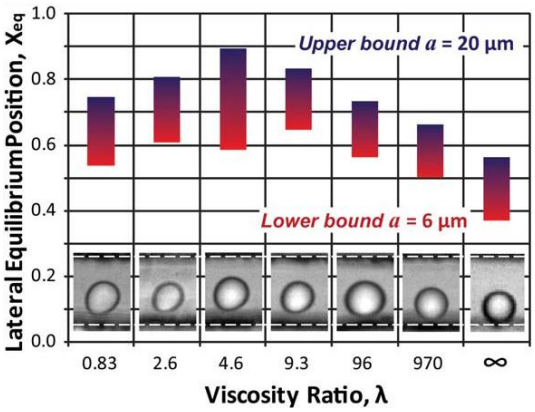

(b) Equilibrium for viscous oil droplets and elastic particles as a function of inner to outer viscosity ratio. The upper to lower bounds of the range is of droplets or particles from 20µm to 6µm.

Figure 3 Extracted from "Deformability-based cell classification and enrichment using inertial microfluidics" by Hur, Soojung Claire and Henderson-MacLennan, Nicole K. and McCabe, Edward R. B. and Di Carlo, Dino, 2011, Lab Chip.

The shapes from figure 3b reflected the extent of deformation regarding the viscosity ratio of

the flow to the viscous oil droplets. An oval is observed from a low viscosity ratio while maintaining a circular shape for a larger viscosity ratio by taking the shape of the cross-section of the droplets and particles. The equilibrium shows a distinctive descend trend after viscosity ratio 9.3. The possible reason for being closer to the channel wall as viscosity decreases below 5 cSt is given by a shift in the direction of deformability-induced migration as a function of the viscosity ratio which has been previously explored by W.Uijttewaal et al. [20] and S.Mortazavi et al. [21]

In this thesis, we would express the deformation of the droplet by using Taylor's small deformation [22] which is defined as the ratio of the difference to the sum of the major and minor axis of the cross-section measured from the plane with streamwise direction and equilibrium direction. We would show that this deformation value could be expressed using dimensionless numbers including Reynolds number, capillary number, dimensionless particle size and viscosity ratio that are the primary components of the problem. This could serve as a useful index for determining the deformation value and enables envisage of a shape of the cell or droplet in a Poiseuille flow. This could be another useful parameter that shows a high correlation to the focusing position of droplets or cells.

1.3 Droplet focusing on lateral sides

The mechanism of inertial focusing is droplets migrating to a place in a microfluidic channel where forces balance with each other. As mentioned previously, the steady state focusing positions for square channel to rectangular channel change from four positions to two positions. The equilibrium positions of flowing particles go could be affected by their initial positions, channel geometry, flow conditions, and particle compliance. Focusing on short sides of the channel has been observed in our experiments and the number of droplets with different migration selection is affected by the flow conditions and particle compliance.

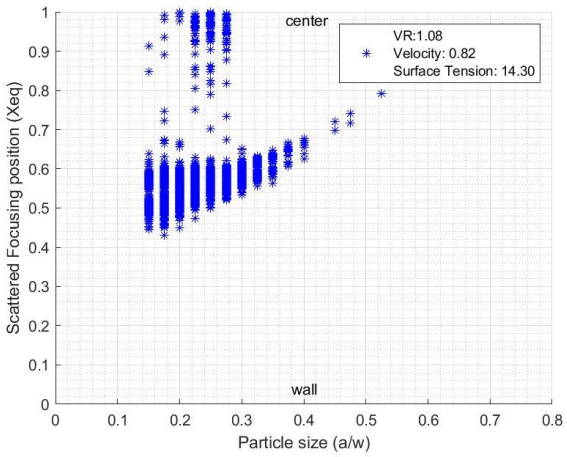

Figure 4 Focusing position scatter plot. Experimental conditions are VR of 1.08, velocity of 0.8m/s and Surface Tension of 14.30N/m. Particle center detected at the center have equilibrium value 1 and 0 at the wall.

From the scatter plot shown in figure 4, there are distinctive two clusters of equilibrium. From the comparison with the results by Hur et al shown in figure 3, the value of equilibrium would be around 0.4 to 0.7 for small particles. This coincides with our results that the lower branch of the clusters is the focusing positions that we intend to detect which depicts the particles focused near the long sides of the channel.

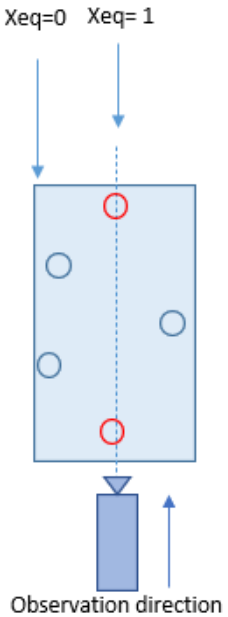

Figure 5 Schematic diagram of inertial focusing.
Droplets in blue are focused at expected positions, droplets in red are focused at lateral sides.

As shown in Figure 5, the detection angle is orthogonal to the plane with the short side and the streamwise direction. It has been nondimensionalized that the Xeq value is 0 when they are near the wall and reaches 1 when they go to the center of the channel. The main area of detection has been accustomed for the particles on the long sides of the channel, where the majority of our particles are focused. Droplets that are focused at the shorter sides are observed to migrate near the center of the wall that they are near to which explains why droplets (in red in Figure 5) would be detected with Xeq value 1.

2 Methodology

2.1 Experimental setup

Droplet preparation and property measurements

Aqueous droplets with various viscosities were prepared using water-in-oil emulsion technique. Viscosity of droplets were systematically varied (1mPas ~ 1.3 Pas) by mixing different weight ratio of glycerol with DI water and measured using a Vibro viscometer (SV-10A, A&D). Fluorinated oils with viscosity of 1.7mPas and 5mPas were used as the continuous phase. Interfacial tension between aqueous and oil phases were varied by adding controlled amount of a surfactant (Krytox 157FSL) and measured using the sessile drop technique.

Inertial focusing of viscous droplets

Oil solutions containing viscous aqueous droplets were injected into a microfluidic channel (60X140μm) with a syringe pump (Harvard Apparatus) to sustain channel Reynolds Number, R_c, between 8 to 50. The diameter, a, deformability, Def, and dynamic lateral position, X_{eq}, were determined using high-speed microscopy (Phantom V1210, Vision Research) and quantified using automated image analysis (MATLAB).

2.2 Dimensionless treatment of results

Dimensionless size

For simplicity, the parameters from our results have been treated dimensionless. The hydraulic droplet diameter is computed by $a = \sqrt{4A/\pi}$ and the sizes have been nondimensionalized by using diameter to channel width (the length of the long side) ratio a/W in which W is the channel width. The dimensionless sizes then have been binned with an interval of 0.025 (droplet sizes 0.35 ± 0.0125 are considered as 0.35) and this is a crucial basis that is used for focusing position and deformation assessment.

Dimensionless equilibrium

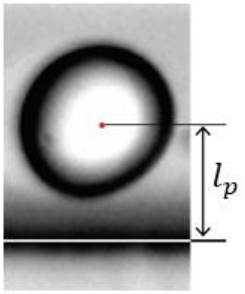

Figure 6 Focusing position detection

As shown in figure 6 the detection of droplet focusing position is also nondimensionalized by dividing it with half of the channel width where $Xeq = l_p/(\frac{W}{2})$. The positions can be expressed concisely as Xeq = 0 is near the wall and Xeq = 1 is near the center.

Dimensionless measured deformation

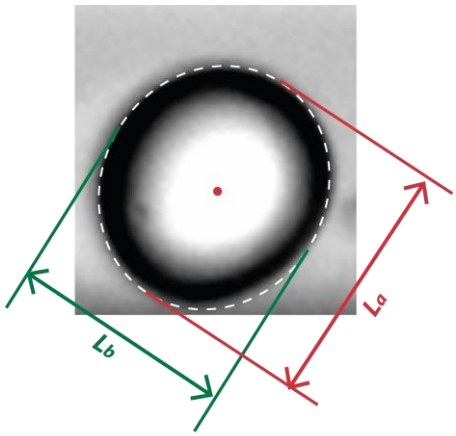

Figure 7 Deformation definition. L_a is the major axis and L_b is the minor axis.

The measured deformation value is calculated by Taylor's deformation where $D = \frac{L_a - L_b}{L_a + L_b}$ as shown in Figure 7. Most of the concerned droplets will form an ellipse shape under high inertial forces, therefore using the ratio of the two axis provides an efficient and simple way of determining the shape of the droplet that we are assessing.

2.3 K-means clustering for determining the droplets for analysis

Figure 4 has shown the scatter plot for one of the experimental conditions. The droplets focused at the shorter sides of the channel are under different forces than that of the ones focused on the

long sides. Due to the difference in the channel length, under no-slip boundary conditions, the distance of maximum velocity in the center would be larger in the lengthwise direction and shorter in the widthwise direction. Therefore, the velocity gradient would be different in the two directions. Because of the limited understanding of the trend of the shorter sides, it is reasonable to analyze the droplets on the longer sides first as they were not only the majority but also covers for larger droplet sizes. It would be shown that for our experimental conditions and channel geometry, only under part of the experimental conditions and droplet size under 0.325 would have this trend.

One way to differentiate particles base on the sides that they are focusing on is using a clustering method to the scatter plot like in figure 4. As compared to using another high-speed camera to detect the equilibrium in the widthwise direction, it provides brevity without having to run the detection procedure twice and linking the same droplets in the videos. Nevertheless, there is no exact threshold for differentiating the two clusters.

K-means clustering [23] is an iterative method that constructs partitions of a data matrix so that the squared Euclidean distance between the row vector for any object and the centroids of its respective clusters is at least as small as the distances to the centroids of the remaining clusters. We are applying K-means clustering on the particles in MATLAB to differentiate droplets focused at two different positions. As the particles with an equilibrium value near 1 are under sizes 0.325, applying K-means clustering on particles under 0.325 would simply the problem that results from the value of the main focusing area being a long and slender shape. The distance is set to ‘sqeuclidean’ and the max iteration is set to ‘1000’ while the rest is the default. There may be controversy to the belong of particles that are in the transitional area as shown in figure 4 but the number of particles in that region is minor compared to the particles of the main focus. This minor error could be neglected in deformation and equilibrium analysis.

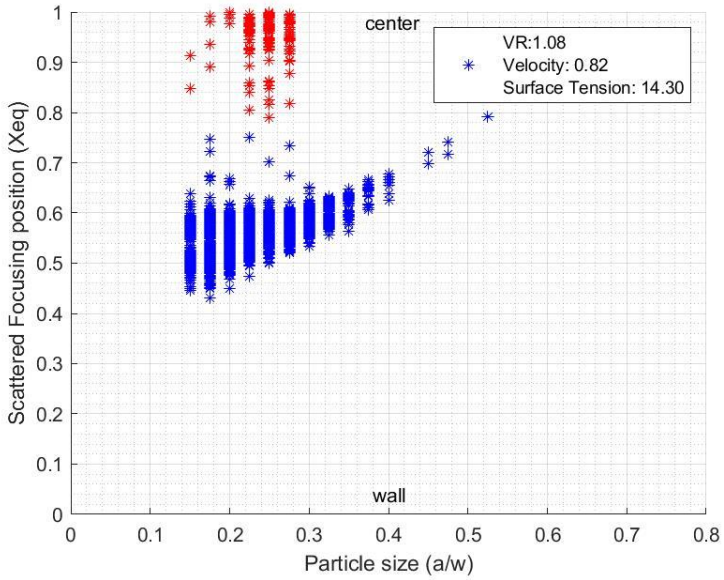

Figure 8 Scatter plot of Figure 4 after applying K-means clustering.

Figure 8 shows the results of what experiment data in figure 4 shows after applying K-means clustering. The red dots are considered focused in the near the short sides and have been excluded from our analysis due to insufficient understanding of this trend. As stated above, few particles that have a slightly larger value than the mainstream are also accounted for but inflict a small impact on the large sample in the mainstream.

3 Results and discussions

3.1 Measured deformation is affected by particle compliance and flow conditions

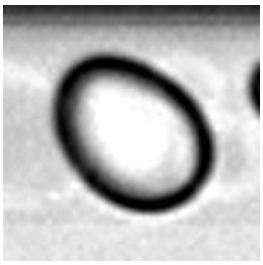

(a) Highly deformed medium particle.

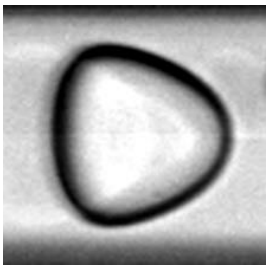

(b) Deformed large particle (a/W >0.4)

Figure 9 Particle with substantial deformation

As compared to the small deformed particle shown in figure 6, figure 9(a) shows the shape of the particle that is under a high flow rate or is highly compliant. The cross-section of the droplet turns into an elliptical shape under high deformation. For droplets of a/W larger than 0.4, rather than forming an elliptical shape, the cross-section of the particle is closer to a triangular shape.

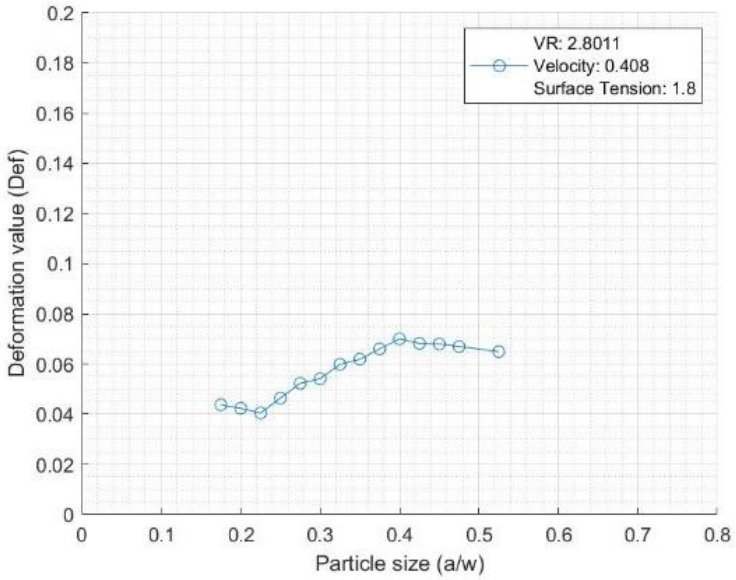

Figure 10 One of a typical line plot of average deformation value to particle size

Figure 10 shows a typical line plot of average deformation value. The deformation for small particles is minor. From the definition of the measured deformation, the accuracy of the numerator $L_a - L_b$ is limited by the resolution for small deformation. The values close to 0 are determined

by the detection code or the irregularity of the circle rather than the difference from the axis of the ellipse. Whereas the value of the denominator $L_a + L_b$ is getting larger for particles from 0.15-0.2, causing the measured deformation value to become smaller. Therefore, in figure 10, we observed a negative slope within particle size 0.175 to 0.225. Large droplets tend to form a triangular shape as shown in Figure 9(b), which results in the drop of measured deformation values. Taking the small or large droplets into account could be inaccurate in characterizing the deformation value. Based on our results, this measurement would be good in revealing the changes of deformation within size 0.2 to 0.4 in which measured deformation value has a monotonic change regarding particle size.

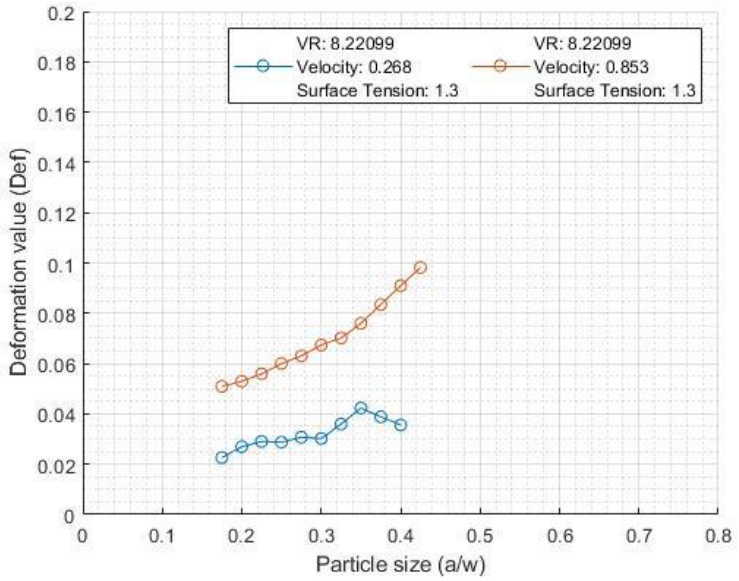

Figure 11a Deformation difference with different velocities. The blue line has a smaller characteristic velocity of 0.268m/s and red of 9.

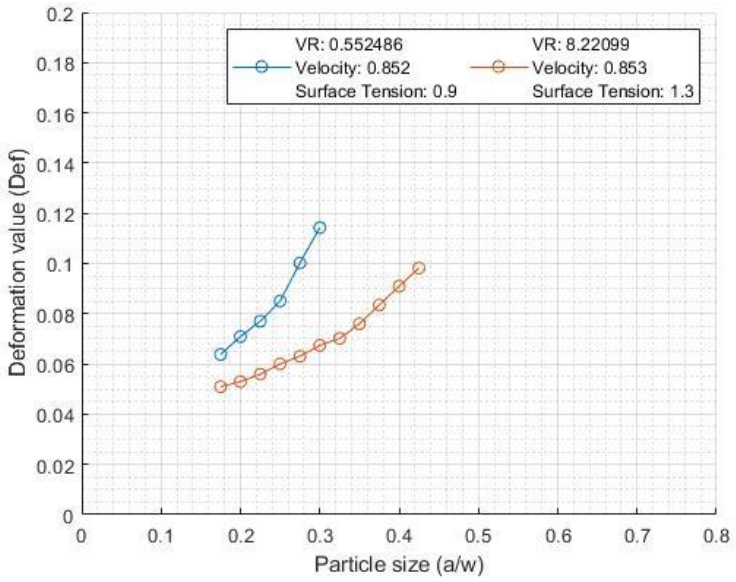

Figure 11b Deformation difference with different viscosity ratios (inner to outer viscosity ratio). The blue line has a smaller VR of 0.55 and red VR of 8.22

Monotonic changes to deformation have been seen for velocity and viscosity ratio. A larger maximum velocity would have a larger velocity gradient, causing a larger shear gradient and deformation of the particle. Therefore, it is intuitive enough to envisage an increase in deformation value regarding velocity as shown in figure 11(a). The viscosity ratio is controlled by the particle viscosity, and particles of small viscosity adopt more deformed shapes coincides with the results from figure 3(b) by Hur et al [17]. One of the comparisons from our experiments is given in figure 11(b).

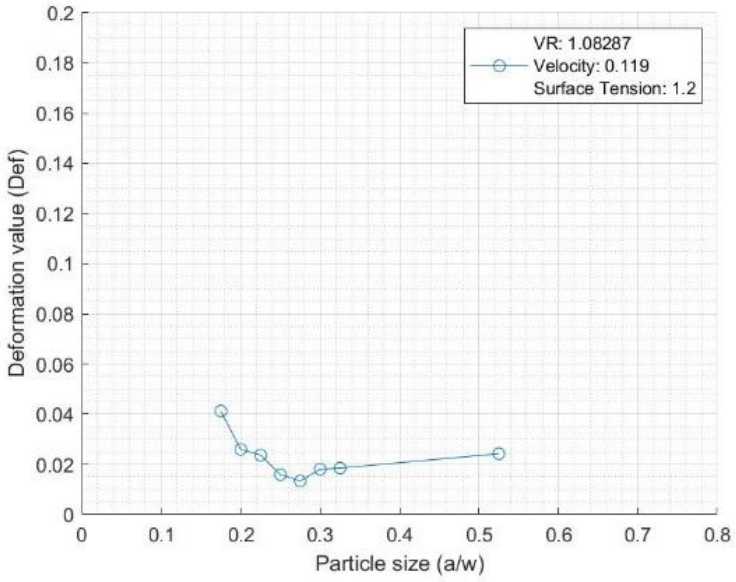

Figure 12 Deformation value under small velocity of 0.119m/s

For conditions where velocities are minor, for instance, the condition shown in Fig.9, reveals an inconsistency to the trend of increased deformation to particle size. Nevertheless, deformation values focused between droplet sizes 0.2 to 0.4 have a deformation value smaller than 0.02, droplets under such a small deformation are affected by detecting accuracy and irregularity of the circle which is similar reasons for the small droplets facing small deformations.

Apart from these low-velocity conditions, Deformation shows a monotonic change towards our experimental variables. This makes the prediction of deformation with these experimental variables applicable using exponential functions.

3.2 Prediction of measured deformation with nonlinear fitting regression

Monotonic trends with experimental variables make way for deformation prediction from the physical properties of the flow and the particle. The equation consists of dimensionless numbers that are decent in characterizing the problem.

$$Deformation = a_0 * Re^{a_1} * VR^{a_2} * (^{a}/_{W})^{a_3} * Ca^{a_4} \quad (1)$$

Nonlinear regression is a form of regression analysis in which observed data are modeled by a function which is a nonlinear combination of the model parameters and depends on one or more independent variables [24]. Equation (1) is the base format that we are fitting into. In which $Re = \rho_c v W/\mu_c$ is Reynolds number and it characterizes the flow conditions; $VR = \mu_d/\mu_c$ is the

viscosity ratio and it characterizes particle compliance control; a/W is dimensionless particle size and $Ca = \mu_c v/\sigma$ is the capillary number that characterizes interfacial interaction for this two-phase problem. Specifically, the input of the size is binned a/W and the independent variable (measured deformation value) for fitting is the average measured deformation value of a binned particle size. The nonlinear fitting regression is performed on MATLAB and the tolerance of the function is set to be 1e-10. This fitting would give us an approximation to our measured deformation.

$$Deformation = 0.0281 * Re^{0.5596} * VR^{-0.1042} * (^{a}/_{W})^{0.8757} * Ca^{0.2941} \quad (2)$$

The predicted deformation equation is given in equation (2). The RMSE of this nonlinear fitting is 0.0112 and the overall R-squared value is 0.8419, indicating that errors are well controlled and overall deformation prediction is decent and applicable.

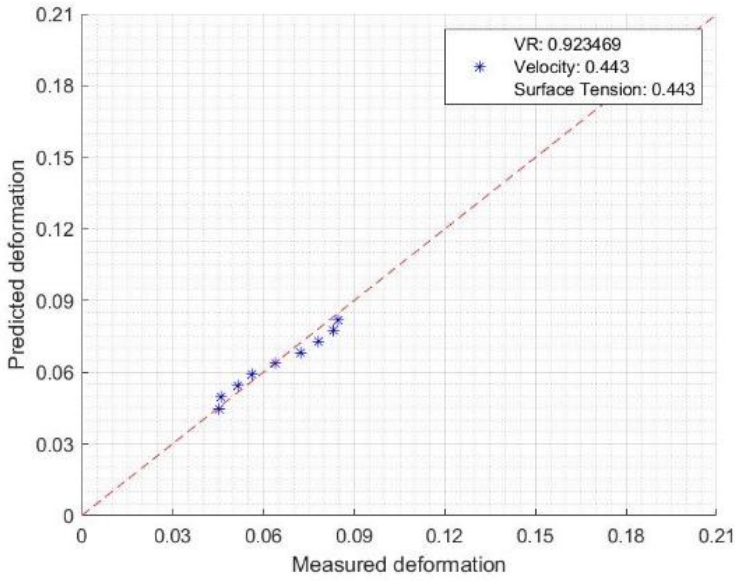

Figure 13 Demonstration of fitting effectiveness

Droplet size would be the main dependent variable under a unique experiment condition. The results are presented by showing the data for one experimental condition, where the curves are depicting the increase of particle size.

Figure 13 shows how measured deformation and predicted deformation using equation (2) works for one of the experiments. The diagonal slope is the line of identicalness for the measured and predicted deformation values. This is one of a typical good fitting and the ascending trend

depicts deformation value change regarding droplet size to the power of 0.8757. The fitting conditions would be discussed in depth later.

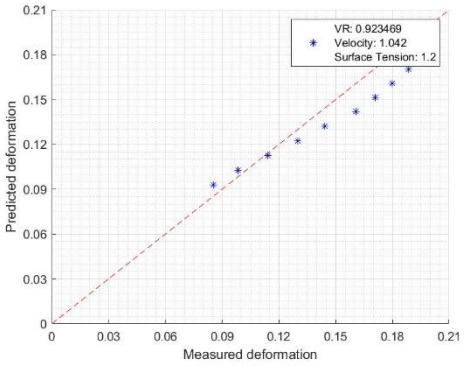

Figure 14(a) Deformation curves under one of the high velocity conditions

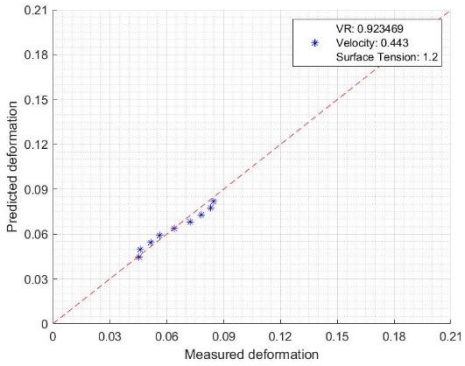

Figure 14(b) Deformation curves under one of the medium velocity conditions

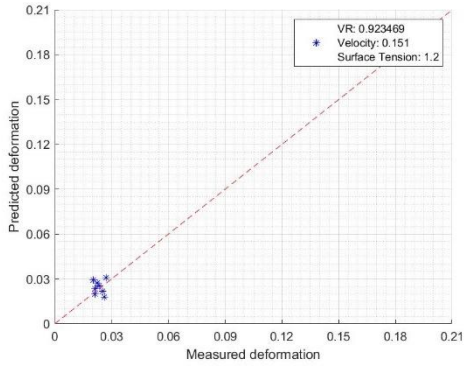

Figure 14(c) Deformation curves under one of the low velocity conditions

Figure 14 shows the effects of velocity on the deformation curves. For low velocities as shown in figure 14(c), droplets are not deformable enough to obey the monotonic change to droplet size, therefore the majority of the low-velocity conditions have data points accumulated below deformation value 0.03. As characteristic velocity reaches larger, the curve starts to show linearity as shown in figure 14(b). The best-fitting accuracy for this region is the best from observations where deformation values lie within the range of 0.03 to 0.1. Figure 14(a) is a high-velocity deformation curve where the average deformation value is larger than 0.07.

Velocity is included in the numerators of both the Reynolds number and Capillary number. The sum of the powers from the two dimensionless numbers is 0.85, indicating that velocity is amplifying the predicted deformation under the power of 0.85. This is a close value to the power of dimensionless particle size and both of the powers are the largest. It suggests that the impact of

velocity and particle size on deformation is the same and largest.

3.3 Goodness of fitting for nonlinear regression

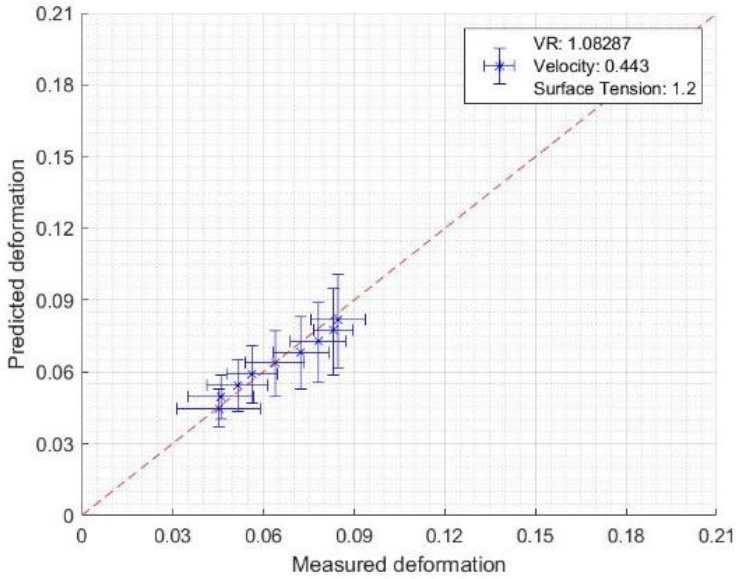

Figure 15 Deformation fitting curve with error bars. The horizontal error bar represents the standard deviation per droplet size. The vertical error bar represents the range of predicted deformation under 95% confidence standard error.

Deformation curves are also assessed with standard deviations of the average deformation per droplet size and standard error of nonlinear fitting regression. The diagonal line or identical line passes through the error box of the majority of our data points which is a verification of having a decent R-squared and RMSE value for data sets in this region.

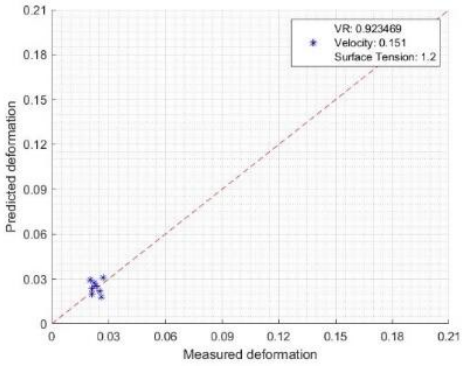

Figure 16(a)

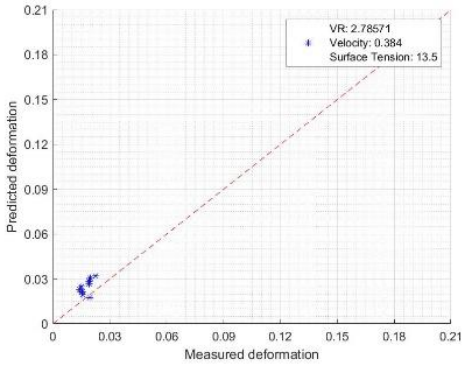

Figure 16(b)

Figure 16 Two low deformation curves

Data points for droplets in low velocity or higher VR environments are in the bottom left corner of the deformation fitting figure as shown in figure 16. Most of the conditions in this region have a characteristic velocity of below 0.3m/s.

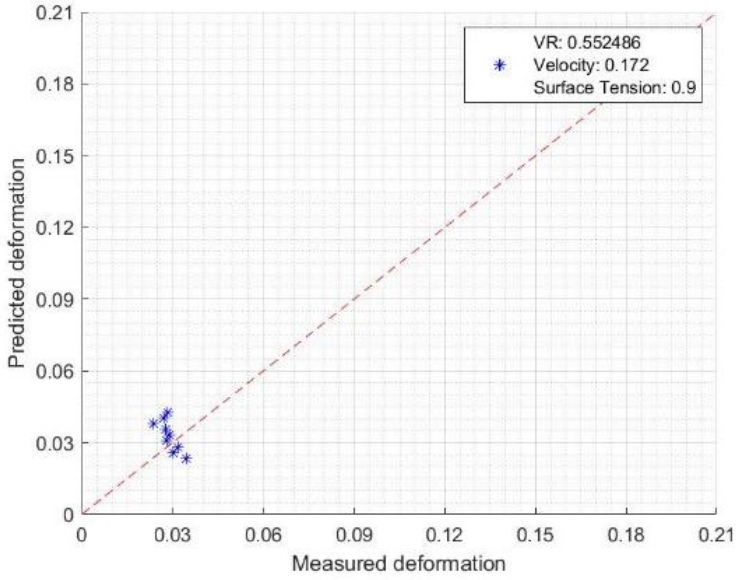

Figure 17 An exception of a small deformation curve

The deformation curve from figure 17 is an interesting exception from our data set. In terms of measured deformation, inertial forces and droplet compliance are still incapable of deforming the particle to a larger extent under this experimental condition. No horizontal alignments indicate that the deformation value does not increase with particle size and the unlike conditions stated in figure 16 that are clustered, it shows a vertical alignment. The combination of small VR and surface tension value makes $VR^{-0.1042} * Ca^{0.2941}$ (equation (2) with only the VR and Ca term) larger and more prone to a/W changes. This suggests corrections may be needed for small VR and surface tension conditions or soft droplets. Nevertheless, small deformation may not be significant in applications as effects would be minor in inertial focusing but future work could be done to find the threshold or the transition to seeing a distinctive ascending trend in deformation with droplet sizes.

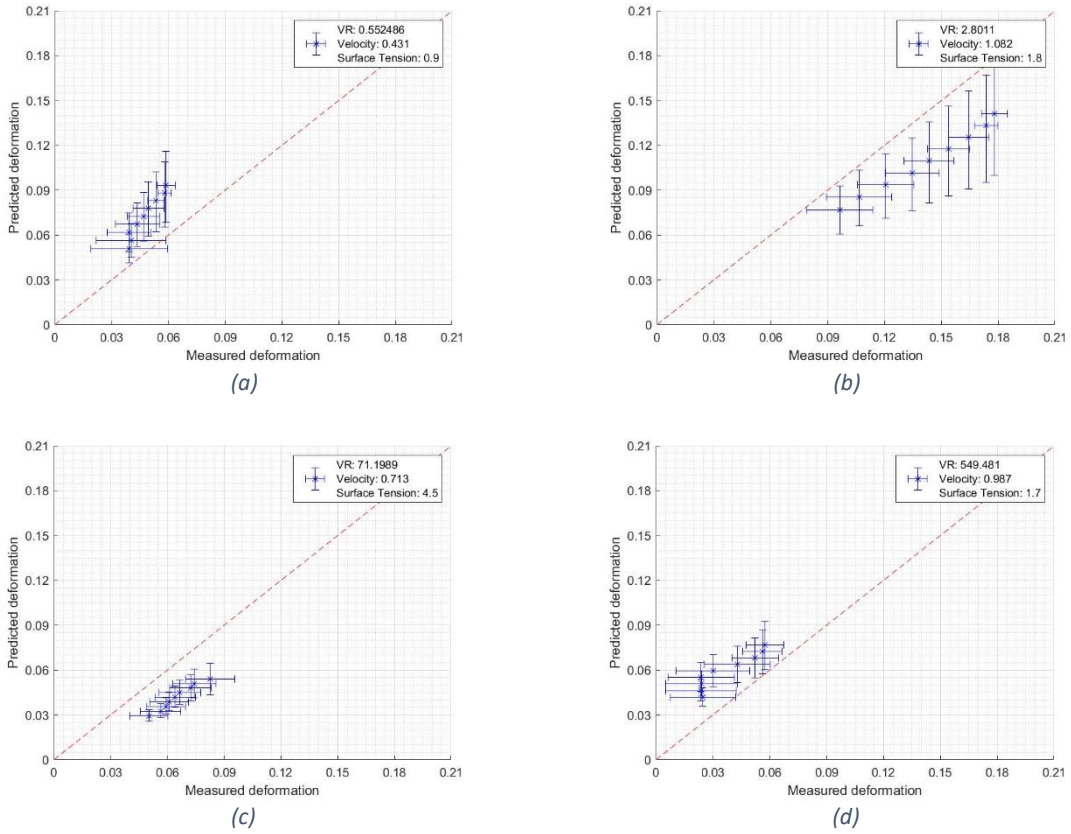

Figure 18 Four exceptions in deformation fitting

For highly deformable particles, adding the errors bars are added into the analysis (error bars are stated under figure 15). Four notable exceptions in deformation fitting are shown in figure 18. Although having a displacement, the slope of the curve is linear and is approximately the same as the diagonal or identical line. That implies have a decent power fitting for the droplet size in equation (2). Of all the data points, major displacements occur in conditions that have smaller surface tension (experiments have two orders of surface tension values). The Capillary number has been enhanced by the power of 3/10 which is nontrivial in the whole term. Surface tension, which is the denominator of the Capillary number, could be a determining factor in this displacement. This suggests that further correction of the power of interfacial forces would be needed for higher accuracy in deformation prediction.

The transition of viscosity ratio is also noteworthy. The viscosity of the droplet characterizes the compliance of the droplet itself. It can value from 0 to infinite representing an inviscid droplet to a rigid droplet. An exponential function provides simplicity and intuitiveness to deformation prediction unbounded for 0 and an infinite VR. This implies that there is a suitable range of

variables that fit well for the above deformation equation.

4 Conclusion

Understanding the mechanisms behind inertial focusing can provide a scientific basis for cell sorting devices. We took an experimental approach to understand how viscoelastic spherical particles deform. From the results, we demonstrated that our deformation definition is decent in characterizing the extent of deformation by particles within sizes 0.2 to 0.4. These droplets form an elliptical shape for their cross-section under deformation. We have also developed an equation including a dimensionless number that are the primary components of the problem. The equation shows decent prediction to the measured deformation value providing a reasonable means of predicting particle deformation with the concerning parameters only.

References

[1] A. A. S. a. K. S. S. a. P. I. Bhagat, "Enhanced particle filtration in straight microchannels using shear-modulated inertial migration," *Physics of Fluids,* p. 101702, 2008.

[2] A. A. S. a. K. S. S. a. P. I. Bhagat, "Inertial microfluidics for continuous particle filtration and extraction," *Microfluidics and nanofluidics,* pp. 217-226, 2009.

[3] J. a. L. M. H. a. K. A. Seo, "Membrane-free microfiltration by asymmetric inertial migration," *Applied Physics Letters,* vol. 91, no. 3, p. 033901, 2007.

[4] A. J. a. D. C. D. Mach, "Continuous scalable blood filtration device using inertial microfluidics," *Biotechnology and bioengineering,* pp. 302-311, 2010.

[5] S. C. a. T. H. T. K. a. D. C. D. Hur, "Sheathless inertial cell ordering for extreme throughput flow cytometry," *Lab on a Chip,* vol. 10, no. 3, pp. 274-280, 2010.

[6] J. a. A. J. R. W. a. A. E. a. C. D. D. a. G. S. W. a. T. M. Oakey, "Particle focusing in staged inertial microfluidic devices for flow cytometry," *Analytical chemistry,* vol. 82, pp. 3862-3867, 2010.

[7] A. A. S. a. K. S. S. a. K. N. a. S. C. J. a. P. I. Bhagat, "Inertial microfluidics for sheath-less high-throughput flow cytometry," *Biomedical microdevices,* vol. 12, no. 2, pp. 187-195, 2010.

[8] Y. a. L. D. a. K. S. A. a. E. J. E. Kang, "DC-Dielectrophoretic separation of biological cells by size," *Biomedical microdevices,* vol. 10, no. 2, pp. 243-249, 2008.

[9] J. Voldman, "Electrical forces for microscale cell manipulation," *Annu. Rev. Biomed. Eng.,* vol. 8, pp. 425-454, 2006.

[10] J. a. X. X. Zhu, "Dielectrophoretic focusing of particles in a microchannel constriction using DC-biased AC flectric fields," *Electrophoresis,* vol. 30, no. 15, pp. 2668-2675, 2009.

[11] A. a. L. T. Lenshof, "Continuous separation of cells and particles in microfluidic systems," *Chemical Society Reviews,* vol. 39, no. 3, pp. 1203-1217, 2010.

[12] N. Pamme, "Continuous flow separations in microfluidic devices," *Lab on a Chip,* vol. 7, no. 12, pp. 1644-1659, 2007.

[13] G. a. S. A. Segre, "Radial particle displacements in Poiseuille flow of suspensions," *Nature,* vol. 189, pp. 209-210, 1961.

[14] B. a. L. A. Chun, "Inertial migration of neutrally buoyant particles in a square duct: An investigation of multiple equilibrium positions," *Physics of Fluids,* vol. 18, no. 3, p. 031704, 2006.

[15] Y.-S. a. S. K.-W. a. L. S.-J. Choi, "Lateral and cross-lateral focusing of spherical particles in a square microchannel," *Lab on a Chip,* vol. 11, no. 3, pp. 460-465, 2011.

[16] C. a. H. G. a. J. X. a. S. J. Liu, "Inertial focusing of spherical particles in rectangular microchannels over a wide range of Reynolds numbers," *Lab on a Chip,* vol. 15, no. 4, pp. 1168-1177, 2015.

[17] S. C. a. H.-M. N. K. a. M. E. R. a. D. C. D. Hur, "Deformability-based cell classification and enrichment using inertial microfluidics," *Lab on a Chip,* vol. 11, no. 5, pp. 912-920, 2011.

[18] S. K. a. B. P. Doddi, "Lateral migration of a capsule in a plane Poiseuille flow in a channel," *International Journal of Multiphase Flow,* vol. 34, no. 10, pp. 966-986, 2008.

[19] C. K. a. H. W. A. Tam, "Transverse motion of an elastic sphere in a shear field," *Journal of Fluid Mechanics,* vol. 58, no. 1, pp. 177-185, 1973.

[20] W. S. a. N. E.-J. a. H. R. M. Uijttewaal, "Droplet migration, deformation, and orientation in the presence of a plane wall: A numerical study compared with analytical theories," *Physics of Fluids A: Fluid Dynamics,* vol. 5, no. 4, pp. 819-825, 1993.

[21] S. a. T. G. Mortazavi, "A numerical study of the motion of drops in Poiseuille flow. Part 1. Lateral migration of one drop," *Journal of Fluid Mechanics,* vol. 411, pp. 325-350, 2000.

[22] E. D. a. T. C. L. Wetzel, "Droplet deformation in dispersions with unequal viscosities and zero interfacial tension," *Journal of Fluid Mechanics,* vol. 426, no. 1, pp. 199--228, 2001.

[23] D. Steinley, "K-means clustering: a half-century synthesis," *British Journal of Mathematical and Statistical Psychology,* vol. 59, no. 1, pp. 1-34, 2006.

[24] "Nonlinear regression," Wikipedia, 16 March 2021. [Online]. Available: https://en.wikipedia.org/wiki/Nonlinear_regression#:~:text=In%20statistics%2C%20nonlinear%20regression%20is,a%20method%20of%20successive%20approximations.. [Accessed 5 5 2021].